arXiv:1610.06780v1 [cond-mat.mes-hall] 21 Oct 2016

Intrinsic exciton states mixing and non-linear optical properties in transition metal dichalcogenide monolayers

M. M. Glazov and L. E. Golub
Ioffe Institute, St. Petersburg 194021, Russia

G. Wang, X. Marie, T. Amand, and B. Urbaszek
Université de Toulouse, INSA-CNRS-UPS, LPCNO, 31077 Toulouse, France

(Dated: October 24, 2016)

Optical properties of transition metal dichalcogenides monolayers are controlled by the Wannier-Mott excitons forming a series of $1s$, $2s$, $2p$, ... hydrogen-like states. We develop the theory of the excited excitonic states energy spectrum fine structure. We predict that p- and s-shell excitons are mixed due to the specific D_{3h} point symmetry of the transition metal dichalcogenide monolayers. Hence, both s- and p-shell excitons are active in both single- and two-photon processes providing an efficient mechanism of second harmonic generation. The corresponding contribution to the nonlinear susceptibility is calculated.

I. INTRODUCTION

Transition metal dichalcogenides monolayers (TMD MLs) such as MoS_2, $MoSe_2$, WS_2, WSe_2, etc., are prototypical two-dimensional (2D) semiconductors with direct band gaps of the order of 2 eV at the Brillouin zone edges [1–5]. Optical properties of these systems are mainly governed by the Coulomb correlated electron-hole pairs, excitons [6, 7]. Due to relatively large effective masses of the electrons and holes and rather weak screening of the Coulomb interaction in 2D systems [8, 9] excitons are highly stable in TMD MLs: The predicted [10–14] and observed [15–20] exciton binding energies amount to $\sim$ 500 meV. The oscillator strengths of excitons in TMD MLs are also much higher as compared with conventional 2D structures based, e.g., on GaAs [21–24]. Just like the direct Coulomb interaction, the electron-hole exchange interaction in TMD MLs is also stronger than in conventional semiconductors [26–29]. It controls the spin and valley dynamics of excitons in a wide range of temperatures [31], see for review Ref. [32] and references therein.

Excitons also play a crucial role in nonlinear optical properties, particularly, in two-photon absorption and second harmonic generation in 2D TMD [16, 18, 20, 33–35]. It is usually assumed that the s-shell exciton states are active in single-photon processes, while p-shell excitons are optically active in two-photon processes [37, 38]. The energies of the ground, $1s$, and excited $2s$, $2p$, ... excitonic states strongly differ from the hydrogenic series due to unusual screening in TMD MLs [17]. Moreover, for the same reason, in TMD MLs the "accidental" Coulomb degeneracy of excited excitonic states is lifted. As a result, the fine structure of the excited, e.g., $2p$-exciton states in TMD MLs has became topical nowadays, in particular, in view of possible manifestations of the Berry curvature effect [39, 40].

Here we demonstrate that the s- and p-shell excitonic states are mixed in TMD monolayers. We present the detailed theory of the fine structure of excited excitonic states in TMD MLs, including the symmetry analysis and the microscopic theory. The microscopic mechanisms of the mixing are uncovered and the detailed model is developed within the $\boldsymbol{k}\cdot\boldsymbol{p}$ formalism. The mixing is shown to be quite substantial, for example, the coupling constant of $2s$- and $2p$-shell states is estimated to be in the range from tenths to several meV. In particular, the mixing makes s-shell states active in the two-photon absorption and also contributes to the second harmonic generation in TMD MLs. The excitonic contributions to the two-photon absorption and nonlinear susceptibility responsible for the second harmonic generation are calculated.

II. SYMMETRY ANALYSIS

The exciton basic wavefunctions in semiconductors can be recast as products of the two-particle envelope and Bloch functions. For the exciton freely propagating in the TMD ML plane with the center of mass wavevector $\boldsymbol{K}$ the wavefunction Ψ reads [32]

$$\Psi_{\boldsymbol{K};\nu,\mu}(\boldsymbol{\rho}_e,\boldsymbol{\rho}_h) = \exp\left(\mathrm{i}\boldsymbol{K}\boldsymbol{R}\right)\Phi_\nu(\boldsymbol{\rho})\mathcal{U}_\mu(\boldsymbol{\rho}_e,\boldsymbol{\rho}_h). \quad (1)$$

The exciton state is characterised by quantum numbers $\nu = 1s, 2s, 2p, \ldots$ denoting the hydrogen-like relative motion states and μ enumerating the band states, respectively, $\Phi_\nu(\boldsymbol{\rho})$ is the relative motion wavefunction and $\mathcal{U}_\mu(\boldsymbol{\rho}_e,\boldsymbol{\rho}_h)$ is the two-particle Bloch function. Here $\boldsymbol{\rho}_e$, $\boldsymbol{\rho}_h$ are the electron and hole in-plane coordinates, respectively, $\boldsymbol{\rho} = \boldsymbol{\rho}_e - \boldsymbol{\rho}_h$ is the relative coordinate, $\boldsymbol{R} = (m_e\boldsymbol{\rho}_e + m_h\boldsymbol{\rho}_h)/(m_e + m_h)$ is the center of mass position vector, m_e (m_h) are the electron (hole) effective masses, the normalization area is set to unity. In what follows we focus on the states with $\boldsymbol{K} = 0$ and restrict ourselves with optically active Bloch states denoted as $\mu = \pm 1$ (active in $\sigma^\pm$ polarizations) or, alternatively, as $\mu = x, y$, where x and y denote orientation of oscillating dipole moment in the Cartesian coordinate frame with the in-plane axes x, y and the normal to the TMD ML z. The "dark" excitons with opposite spins of the

electron and the hole which are weakly optically active in the polarization perpendicular to the ML plane are disregarded [26, 41].

The point symmetry of the TMD ML is D_{3h}, in the chosen coordinate frame z is the three-fold rotation axis and y is (one of three) two-fold in-plane rotation axes, the horizontal reflection plane $\sigma_h \parallel (xy)$, one of three vertical reflection planes is $\sigma_v \parallel (yz)$ and two remaining planes can be obtained from σ_v by the rotation through the angles $\pm 2\pi/3$ around z-axis. The set of axis and atomic arrangement is illustrated in Fig. 1. In accordance with the general theory, the exciton eigenstates in TMD ML transform according to irreducible representations of the D_{3h} point group [37].

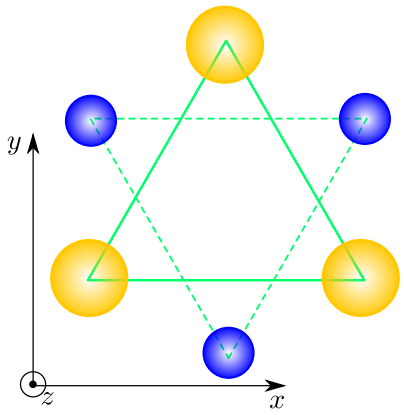

Figure 1. Top view of atomic arrangement in TMD ML. Yellow circles show positions of the transition metal atoms, blue circles show the projection of chalcogen atoms on the horizontal plane. Green lines are guides for eye showing non-equivalent triangles responsible for the overall D_{3h} point symmetry of the ML.

The symmetry of exciton basic state is, in accordance with Eq. (1), described by the product of irreducible representations corresponding to the relative motion wavefunction and Bloch function. Noteworthy that the symmetry of the two-dimensional envelope function $\Phi_\nu(\boldsymbol{\rho})$ can be either A_1' or Γ_1 in the notations of Ref. [42] (the identical representation, s-shell) or E' or Γ_6 (the in-plane vector components, p-shells). In fact, all other 2D hydrogen-like states transform by reducible representations being combinations of those two, for instance, d-shell excitonic states (with the angular momentum z-component being ± 2) transform according to E', because in the D_{3h} point symmetry the pair of coordinates (x, y) transform exactly as the second-order combinations $(2xy, x^2 - y^2)$. The Bloch functions $\mathcal{U}_{x,y}$ of the optically active states transform according to the two-dimensional irreducible representation E'. Hence, with account for the Bloch function, the s-shell excitons transform according to the irreducible two-dimensional representation

$$\mathcal{D}_s = A_1' \times E' = E', \tag{2}$$

while p-shell excitonic states transform according to the reducible representation

$$\mathcal{D}_p = E' \times E' = A_1' + A_2' + E'. \tag{3}$$

Equation (3) demonstrates that with account for the point symmetry of TMD ML the p-shell quadruplet is split into two non-degenerate sublevels (A_1', A_2') and the two-fold degenerate level E' with the eigenfunctions (the normalization constants are omitted for brevity):

$$A_1': \quad \Phi_{p_x}\mathcal{U}_x + \Phi_{p_y}\mathcal{U}_y, \tag{4a}$$
$$A_2': \quad \Phi_{p_x}\mathcal{U}_y - \Phi_{p_y}\mathcal{U}_x, \tag{4b}$$
$$E'\ (1): \quad \Phi_{p_x}\mathcal{U}_y + \Phi_{p_y}\mathcal{U}_x, \tag{4c}$$
$$E'\ (2): \quad \Phi_{p_x}\mathcal{U}_x - \Phi_{p_y}\mathcal{U}_y. \tag{4d}$$

The splitting between the $2p$ states transforming according to E' and $(A_1' + A_2')$ was discussed in Refs. [38–40, 43], while the splitting between A_1' and A_2' as well as the mixing between s-shell and p-shell states, see below, was not addressed. The fine structure of p-shell exciton states is illustrated in Fig. 2 for the particular example of $2p$ excitons. The basic functions (4) can be represented in the alternative form in the basis of the states with a given angular momentum z-component ± 1 as $\Phi_{p_{+1}}\mathcal{U}_{-1} \pm \Phi_{p_{-1}}\mathcal{U}_{+1}$ where the top (bottom) sign corresponding to A_1' (A_2') irreducible representation, and $\Phi_{p_{+1}}\mathcal{U}_{+1}$, $\Phi_{p_{-1}}\mathcal{U}_{-1}$ for two basic functions of E' irreducible representation. The latter functions formally correspond to the total angular momentum component being ± 2 and, since the three-fold rotation leaves third angular harmonics invariant, these functions transform exactly as the states with the angular momentum components ∓ 1, respectively. The states A_1' and A_2' are, respectively, symmetrized and antisymmetrized combinations of the basic functions with the total angular momentum component being 0.

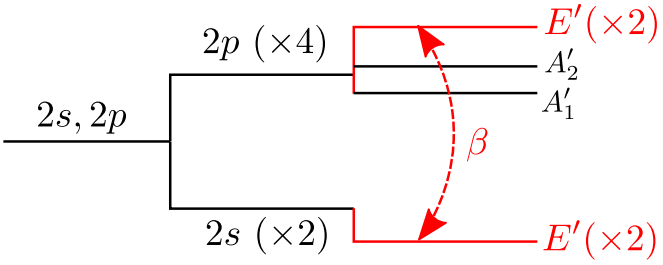

Figure 2. Sketch of the $2s$ and $2p$-shell exciton fine structure. The splitting between the $2p$ quadruplet and $2s$ doublet (with account for the Bloch functions orbital degeneracy) arises due to the specific screening of the Coulomb interaction in TMD MLs. The splitting of the $2p$ quadruplet arises in D_{3h} point symmetry and the $2p$ (E') states are mixed with the $2s$ (E') states. The order of lines is arbitrarily and the splittings are shown not to scale.

Moreover, it follows from Eqs. (2) and (3) that the s-shell excitonic states and the combinations Eqs. (4c), (4d) of the p-shell states transform according to the same irreducible representation E' of the D_{3h} point group. Therefore, the mixing of these states is possible. In particular,

the p-shell state combination $\Phi_{p_x}\mathcal{U}_x - \Phi_{p_y}\mathcal{U}_y$ mixes with $\Phi_s\mathcal{U}_y$ and the $\Phi_{p_x}\mathcal{U}_y + \Phi_{p_y}\mathcal{U}_x$ mixes with $\Phi_s\mathcal{U}_x$. In the basis of the states with given components of the total angular momentum the mixing involves the pairs:

$$\Phi_{p_{+1}}\mathcal{U}_{+1} \leftrightarrow \Phi_s\mathcal{U}_{-1}, \quad \Phi_{p_{-1}}\mathcal{U}_{-1} \leftrightarrow \Phi_s\mathcal{U}_{+1}. \tag{5}$$

This mixing makes p-shell states optically active. For given principal quantum numbers n and m of the s- and p-shell states the mixing is described by a single parameter β_{nm}. To illustrate this mixing in more detail we focus on the states with the principal quantum numbers $n = m = 2$. We note that for purely Coulomb potential the $2s$ and $2p$ levels are degenerate. This so-called "accidental" degeneracy is lifted for the effective electron-hole interaction potential in TMD ML which accounts for specifics of the screening [38]. The spin-orbit interaction as well as non-parabolicity of the single-particle energy spectrum can also contribute to the s-p exciton splitting. To the best of our knowledge this expected splitting has not been measured so far. The effective Hamiltonian of $2s/2p$ excitons can be represented as:

$$\mathcal{H}_{2X} = \begin{pmatrix} E_{2s} & 0 & 0 & 0 & \beta & 0 \\ 0 & E_{2s} & 0 & 0 & 0 & \beta \\ 0 & 0 & E_{2p}^{(A_1')} & 0 & 0 & 0 \\ 0 & 0 & 0 & E_{2p}^{(A_2')} & 0 & 0 \\ \beta & 0 & 0 & 0 & E_{2p}^{E'} & 0 \\ 0 & \beta & 0 & 0 & 0 & E_{2p}^{E'} \end{pmatrix}. \tag{6}$$

Here the basic functions are chosen in the following order: $2s; E'(1)$, $2s; E'(2)$, $2p; A_1'$, $2p; A_2'$, $2p; E'(1)$ $2p; E'(2)$, the diagonal energies E_{2s}, $E_{2p}^{A_1'}$, etc. denote exciton energies neglecting the s-p mixing, and $\beta \equiv \beta_{22}$ is the mixing parameter. Obviously, the effective Hamiltonians for the multiplets with different principal quantum numbers have the same form with different values of parameters, the mixing is symmetry allowed between any n and m.

III. MICROSCOPIC ORIGIN OF s-p EXCITON MIXING

In this section we develop the microscopic model of the s-p exciton mixing. The splitting of s-shell and p-shell excitonic states for the given principal quantum number n has been discussed in literature in detail, see Ref. [38] and references therein. The E' doublet of p-shell states and the two states A_1', A_2' are split as a result of the $\boldsymbol{k}\cdot\boldsymbol{p}$-interaction and the band mixing [39, 40]. This splitting as well as the splitting between A_1' and A_2' p-shell excitons (studied for axially-symmetric quantum dots in Ref. [44]) is allowed in the axially symmetric model and it does not rely on specific features of the TMD symmetry and band structure. By contrast, the mixing of the p- and s-shell states requires accounting for the symmetry reduction from the axial down to the three-fold symmetry. Note that in TMD MLs the bright exciton Bloch function involves the electron state in $\boldsymbol{K}_\pm$ valley and the hole state in the $\boldsymbol{K}_\mp$ valley, see Ref. [32] and the text below for details. Therefore, since the mixing involves the pairs, Eq. (5), where the electron and hole in the initial and final states should swap valleys, the coupling between p- and s-shell excitons is a combined effect of the $\boldsymbol{k}\cdot\boldsymbol{p}$-mixing of the energy bands and the electron-hole interaction. Both the short- and long-range parts of the electron-hole exchange interaction may enable simultaneous intervalley transfer of the electron and the hole [26, 27]. Below we calculate two contributions to the mixing parameter $\beta = \beta_s + \beta_l$ related with both exchange interaction mechanisms: the short range contribution, β_s, in Sec. III B and the long-range one, β_l, in Sec. III C.

In what follows we present the model of the exciton mixing based on the following steps. First, we introduce the envelope functions $\Phi_\nu(\boldsymbol{\rho})$, which can be calculated within the effective mass method as, e.g., in Ref. [17]. Second, we take into account the first-order $\boldsymbol{k}\cdot\boldsymbol{p}$ mixing between the different bands, which results in the mixing of the s- and p-shell excitonic states within a given valley. Third, the short- and long-range parts of the exchange interaction are taken into account to derive the mixing between the excitons in different valleys.

A. Exciton wavefunction

We are interested in the excitons formed by the single-particle Bloch states in the vicinity of the $\boldsymbol{K}_\pm$ edges of the Brillouin zone. Neglecting the Coulomb-interaction induced band mixing the two-particle Bloch function $\mathcal{U}_\mu(\boldsymbol{\rho}_e, \boldsymbol{\rho}_h)$ can be presented as a product of the electron and hole Bloch functions. For the excitonic state active in σ^+ polarization, $\mu = +1$, the electron Bloch state corresponds to the conduction band c in the $\boldsymbol{K}_+$ valley and the hole state in the valence band v in the $\boldsymbol{K}_-$ valley, because the hole state is obtained from the empty state in the valence band by the time-reversal operation [32, 37]. Within the $\boldsymbol{k}\cdot\boldsymbol{p}$ model the Coulomb interaction induces the admixture of the remote bands due to the real space localization of the envelope function and, correspondingly, its spread in the reciprocal, $\boldsymbol{k}$-space. We resort to the standard $\boldsymbol{k}\cdot\boldsymbol{p}$ model presented in Refs. [45–47] which adequately describes the D_{3h} point symmetry of the TMD ML and includes several nearest bands in agreement with DFT calculations. Disregading spin and neglecting the spin-orbit interaction we choose the basis functions for the bands $c+2, c, v, v-3$ (see Ref. [46] for notations) in the $\boldsymbol{K}_+$ valley as follows:

$$\mathcal{U}_{c+2}^{(+)} = \frac{\mathcal{X} - \mathrm{i}\mathcal{Y}}{\sqrt{2}}, \quad \mathcal{U}_c^{(+)} = \frac{\mathcal{X} + \mathrm{i}\mathcal{Y}}{\sqrt{2}}, \tag{7}$$

$$\mathcal{U}_v^{(+)} = \mathcal{S}, \quad \mathcal{U}_{v-3}^{(+)} = \frac{\mathcal{X} - \mathrm{i}\mathcal{Y}}{\sqrt{2}}.$$

Here the subscript refers to the band, the superscript denotes the valley, and the arguments are omitted for brevity; the functions $\mathcal{X}$, $\mathcal{Y}$ transform as the coordinates x and y, respectively, the function $\mathcal{S}$ is invariant. One can see that the valence band, v, is invariant under the point-group transformations of TMD ML, the conduction band, c, transforms as the state with the angular momentum z-component being equal to $+1$, and the remote valence and conduction bands, $v-3$ and $c+2$, respectively, transform as the states with the angular momentum component being -1. The $\boldsymbol{K}_-$ valley states are related to the $\boldsymbol{K}_+$ states by the time-reversal operation, therefore the orbital Bloch functions in $\boldsymbol{K}_-$ valley can be obtained by the complex conjugation of the functions Eq. (7). The effective Hamiltonian for the K_+ valley in the electron representation has the following form:

$$\mathcal{H}_+ = \begin{pmatrix} E_{c+2} & \gamma_6 k_- & \gamma_4 k_+ & 0 \\ \gamma_6^* k_+ & E_c & \gamma_3 k_- & \gamma_5 k_+ \\ \gamma_4^* k_- & \gamma_3^* k_+ & E_v & \gamma_2 k_- \\ 0 & \gamma_5^* k_- & \gamma_2^* k_+ & E_{v-3} \end{pmatrix}, \tag{8}$$

and in the K_- valley the Hamiltonian is obtained by the substitution [46]

$$\gamma_i \to \gamma_i^*, \qquad k_\pm \to -k_\mp. \tag{9}$$

Here $\gamma_2, \ldots \gamma_6$ are the constants related with the interband matrix elements of the momentum operator, $k_\pm = k_x \pm \mathrm{i}k_y$ are the cyclic components of the wavevector operator $\boldsymbol{k} = -\mathrm{i}\partial/\partial\boldsymbol{\rho}_e$ reckoned from the Brillouin zone edge. The diagonal terms $\propto k^2$ caused by the free-electron dispersion and distant bands contributions are disregarded. Note that if we choose all orbitals $\mathcal{S}, \mathcal{X}, \mathcal{Y}$ to be real, then all γ parameters are purely imaginary. The Hamiltonian in the hole representation is obtained from Eq. (8) by the time-reversal operation, see Ref. [36] for details.

In the first order in the $\boldsymbol{k}\cdot\boldsymbol{p}$ mixing of the conduction and valence bands with the $c+2$ and $v-3$ bands we obtain the wavefunctions of the excitons $\Psi_{\mathbf{0};\nu;\pm1}$ in the form

$$\Psi_{\mathbf{0};\nu;\pm1} = \Phi_\nu(\boldsymbol{\rho})\mathcal{U}_\pm(\boldsymbol{\rho}_e,\boldsymbol{\rho}_h) + \left[\hat{k}_\mp \Phi_\nu(\boldsymbol{\rho})\right] \mathcal{W}_\mp(\boldsymbol{\rho}_e,\boldsymbol{\rho}_h) + \ldots. \tag{10}$$

Here $\ldots$ denote omitted terms related with the $\boldsymbol{k}\cdot\boldsymbol{p}$ mixing of the c and v bands as well as with the distant bands beyond the $c+2$, $v-3$, these terms are not important for the following,

$$\left[\hat{k}_\mp \Phi_\nu(\boldsymbol{\rho})\right] = -\mathrm{i}\left(\partial/\partial x \mp \mathrm{i}\partial/\partial y\right)\Phi_\nu(\boldsymbol{\rho}),$$

the two-particle Bloch functions

$$\mathcal{U}_\pm(\boldsymbol{\rho}_e,\boldsymbol{\rho}_h) = \mathcal{U}_c^{(\pm)}(\boldsymbol{\rho}_e)\tilde{\mathcal{U}}_v^{(\mp)}(\boldsymbol{\rho}_h), \tag{11}$$

where the tilde on top means that the Bloch function is taken in the hole representation [32, 36, 37], and the auxiliary combinations of Bloch functions are derived within the first-order perturbation theory as

$$\mathcal{W}_- = \left(\frac{\gamma_6 \mathcal{U}_{c+2}^{(+)}(\boldsymbol{\rho}_e)}{E_c - E_{c+2}} + \frac{\gamma_5^* \mathcal{U}_{v-3}^{(+)}(\boldsymbol{\rho}_e)}{E_c - E_{v-3}}\right)\tilde{\mathcal{U}}_v^{(-)}(\boldsymbol{\rho}_h) + \mathcal{U}_c^{(+)}(\boldsymbol{\rho}_e)\left(\frac{\gamma_4^* \tilde{\mathcal{U}}_{c+2}^{(-)}(\boldsymbol{\rho}_h)}{E_v - E_{c+2}} + \frac{\gamma_2 \tilde{\mathcal{U}}_{v-3}^{(-)}(\boldsymbol{\rho}_h)}{E_v - E_{v-3}}\right), \tag{12a}$$

$$\mathcal{W}_+(\boldsymbol{\rho}_e,\boldsymbol{\rho}_h) = -\left(\frac{\gamma_6^* \mathcal{U}_{c+2}^{(-)}(\boldsymbol{\rho}_e)}{E_c - E_{c+2}} + \frac{\gamma_5 \mathcal{U}_{v-3}^{(-)}(\boldsymbol{\rho}_e)}{E_c - E_{v-3}}\right)\tilde{\mathcal{U}}_v^{(+)}(\boldsymbol{\rho}_h) - \mathcal{U}_c^{(-)}(\boldsymbol{\rho}_e)\left(\frac{\gamma_4 \tilde{\mathcal{U}}_{c+2}^{(+)}(\boldsymbol{\rho}_h)}{E_v - E_{c+2}} + \frac{\gamma_2^* \tilde{\mathcal{U}}_{v-3}^{(+)}(\boldsymbol{\rho}_h)}{E_v - E_{v-3}}\right). \tag{12b}$$

Note that the first lines of Eqs. (12a), (12b) result from the $\boldsymbol{k}\cdot\boldsymbol{p}$-mixing of the electron states while the second lines in Eqs. (12a), (12b) result from the $\boldsymbol{k}\cdot\boldsymbol{p}$-mixing of the hole states, see Appendix A for the details of derivation. The functions $\mathcal{W}_\pm$ transform, under operations from D_{3h} point group, as the functions with angular momentum components ±1. Equation (10) illustrates that the states with the angular momentum components ±1 and ∓2 are indistinguishable in D_{3h} point symmetry. This expression already describes the mixing of excitonic states with different parity, particularly, s- and p-shell states within the same valley.

The mixing is schematically shown in Fig. 3 by the example of the $2p_+$ exciton formed from the electron in the $\boldsymbol{K}_+$ valley, $\Psi_{\mathbf{0};2p_+;+1}$ (panel a), and the $2s$ exciton formed from the electron in the $\boldsymbol{K}_-$ valley, $\Psi_{\mathbf{0};2s;-1}$ (panel b). The mixing of the conduction band with the $c+2$ band is shown and the modification of the envelopes $\Phi_{2p_+} \to \Phi_s$ and $\Phi_{2s} \to \Phi_{p_+}$ described by Eq. (10) is sketched. We stress that symmetry-wise the functions demonstrated on the panels (a) and (b) are equivalent.

B. Short-range interaction

Our ultimate goal is to describe the mixing of the $\Psi_{\mathbf{0};2p_+,+1}$ and $\Psi_{\mathbf{0};2s,-1}$ where the electrons belong to different valleys. Such mixing can be enabled by the electron-hole Coulomb interaction. Particularly, its short range part is responsible for the simultaneous intervalley transfer of individual charge carriers forming an exciton. Indeed, as it follows from Eqs. (12) the exciton Bloch functions combinations $\mathcal{W}_\pm$ transform exactly as $\mathcal{U}_\pm$ exciton Bloch functions under all D_{3h} point group transformations. We present the effective Hamiltonian of the short-range electron-hole interaction in the standard form [37]:

$$\mathcal{H}_{sr} = \delta(\boldsymbol{\rho}_e - \boldsymbol{\rho}_h)\,\mathcal{E}_0 a_0^2\,\hat{V}, \tag{13}$$

where the Dirac δ-function, $\delta(\boldsymbol{\rho}_e - \boldsymbol{\rho}_h)$, acts on the smooth envelopes, $\mathcal{E}_0$ and a_0 are the "atomic" energy

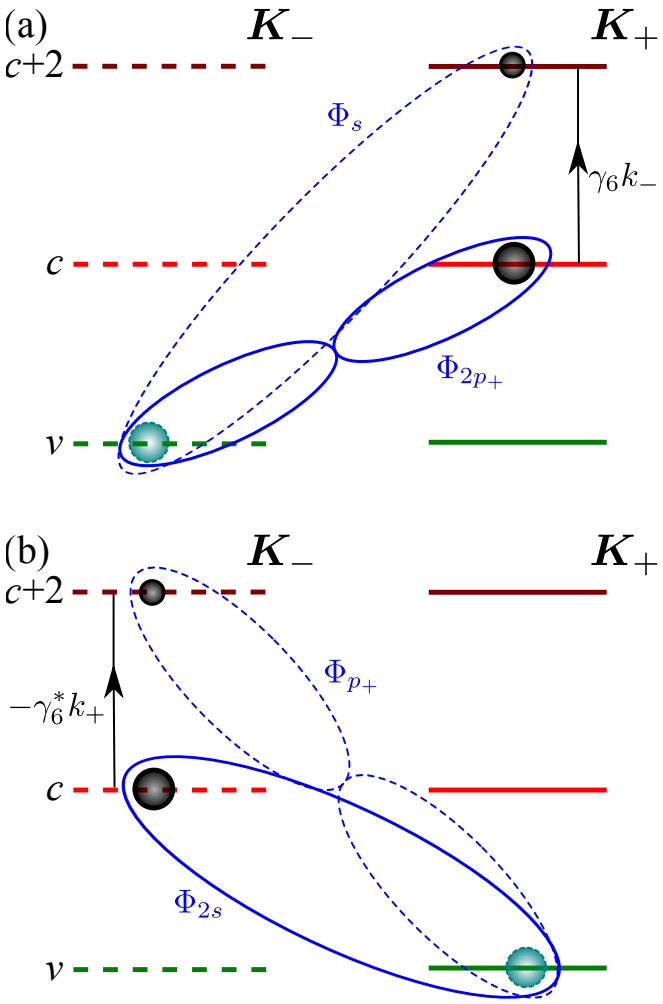

Figure 3. Schematic illustration of the exciton states mixing within the same valley, Eqs. (10), (12). We used here hole representation for the valence band states. (a) The admixture of s-shell state to $2p_+$ state in $\boldsymbol{K}_+$ in $\Psi_{\mathbf{0};2p_+;+1}$. (b) The admixture of the p_+-state to the s-shell state in $\boldsymbol{K}_-$ valley, $\Psi_{\mathbf{0};2s;-1}$. Black circles denote electron states, green circles denote hole states, blue solid and dashed lines denote the envelope functions: 8-like shape for p-shell and elliptical for s-shell. Vertical arrows denote the matrix elements of $\boldsymbol{k}\cdot\boldsymbol{p}$ Hamiltonians $\mathcal{H}_\pm$ between c and $c+2$ states.

scale and the lattice constant, respectively, and the dimensionless matrix $\hat{V}$ acts in the basis of two-particle Bloch functions. It has nonzero elements between the exciton Bloch functions of the same symmetry, e.g., $\langle \mathcal{U}_{c+2}^{(-)}\tilde{\mathcal{U}}_v^{(+)}|\hat{V}|\mathcal{U}_c^{(+)}\tilde{\mathcal{U}}_v^{(-)}\rangle$. Also, taking into account the spin and the spin-orbit interaction, the short-range exchange between the electron and the hole enables simultaneous flip-flop of the electron and hole spins giving rise to the mixing of s-shell and p-shell excitons of the A-series.

The calculation shows that the s-p exciton mixing constant β in the Hamiltonian (6) reads

$$\beta_s = \mathcal{E}_0 a_0^3 \Phi_{2s}^*(0)\Phi'_{2p}(0) B_s, \tag{14}$$

where we introduced the notations

$$\Phi'_{2p}(\rho) = \left(\frac{\partial}{\partial x} - \mathrm{i}\frac{\partial}{\partial y}\right)\Phi_{2p_+} = \left(\frac{\partial}{\partial x} + \mathrm{i}\frac{\partial}{\partial y}\right)\Phi_{2p_-}, \tag{15}$$

and the dimensionless parameter

$$B_s = -\frac{1}{a_0}\left(\frac{\gamma_6\langle \mathcal{U}_c^{(-)}\tilde{\mathcal{U}}_v^{(+)}|\hat{V}|\mathcal{U}_{c+2}^{(+)}\tilde{\mathcal{U}}_v^{(-)}\rangle}{E_c - E_{c+2}} + \frac{\gamma_5^*\langle \mathcal{U}_c^{(-)}\tilde{\mathcal{U}}_v^{(+)}|\hat{V}|\mathcal{U}_{v-3}^{(+)}\tilde{\mathcal{U}}_v^{(-)}\rangle}{E_c - E_{v-3}} + \frac{\gamma_4^*\langle \mathcal{U}_c^{(-)}\tilde{\mathcal{U}}_v^{(+)}|\hat{V}|\mathcal{U}_c^{(+)}\tilde{\mathcal{U}}_{c+2}^{(-)}\rangle}{E_v - E_{c+2}} + \frac{\gamma_2\langle \mathcal{U}_c^{(-)}\tilde{\mathcal{U}}_v^{(+)}|\hat{V}|\mathcal{U}_c^{(+)}\tilde{\mathcal{U}}_{v-3}^{(-)}\rangle}{E_v - E_{v-3}}\right). \tag{16}$$

Physically, the parameter B_s accounts for the trigonality on the level of Bloch functions. For estimates we obtain from Eq. (14) the short-range contribution to the mixing constant $\beta_s \sim \mathcal{E}_0(a_0/a_B)^3 B_s$, where a_B is the exciton Bohr radius. As a result, for $\mathcal{E}_0 = 1$ eV, $a_0 = 3$ Å, $a_B = 15$ Å, we have β_s in the range from several tenths to several meV for B_s ranging from 0.1 to 1. In the same way one may roughly estimate the short-range contribution to the s-shell exciton energy, $\sim \mathcal{E}_0(a_0/a_B)^2$ is on the order of 10 meV, in reasonable agreement with microscopic calculations [29, 30].

C. Exciton oscillator strengths and the long-range exchange interaction

As stated above the s-p mixing can have a second contribution due to the long-range exchange interaction. The s-shell excitons formed with electrons in $\boldsymbol{K}_\pm$ valley are optically active in $\sigma^\pm$ polarizations [48, 49]. These selection rules are described by the dipole moment operator. The reduced matrix elements of the light-matter interaction, $-(\hat{d}_\pm e_\mp)$, where $\hat{d}_\pm = (\hat{d}_x \pm \mathrm{i}\hat{d}_y)/\sqrt{2}$, $e_\pm = (e_x \pm \mathrm{i}e_y)/\sqrt{2}$ are the circular components of the dipole moment operator and of polarization vector, respectively, can be recast as

$$\langle \Psi_{\mathbf{0};ns;+1}| - (\hat{d}_+ e_-)|0\rangle = -\frac{\mathrm{i}\sqrt{2}e}{E_{ns}}\Phi_{ns}^*(0)\gamma_3 e_-, \tag{17a}$$

$$\langle \Psi_{\mathbf{0};ns;-1}| - (\hat{d}_- e_+)|0\rangle = +\frac{\mathrm{i}\sqrt{2}e}{E_{ns}}\Phi_{ns}^*(0)\gamma_3^* e_+, \tag{17b}$$

where E_ν is excitation energy of νth exciton. It follows from Eqs. (10) and (12) that the $p_\pm$-shell excitons formed with electrons in $\boldsymbol{K}_\pm$ valley are also optically active, but in the opposite, $\sigma^\mp$, polarizations. The matrix elements of the dipole moment operator evaluated in the first-order in $\boldsymbol{k}\cdot\boldsymbol{p}$ interaction with remote $c+2$, $v-3$ bands take

the form

$$\langle\Psi_{\mathbf{0};np_+;+1}|-(\hat{d}_-e_+)|0\rangle=-\frac{\mathrm{i}\sqrt{2}e}{E_{np}}\left[\Phi'_{np}(0)\right]^*\gamma_3 A, \tag{18a}$$

$$\langle\Psi_{\mathbf{0};np_-;-1}|-(\hat{d}_+e_-)|0\rangle=+\frac{\mathrm{i}\sqrt{2}e}{E_{np}}\left[\Phi'_{np}(0)\right]^*\gamma_3^* A^*, \tag{18b}$$

where

$$A=\frac{1}{\mathrm{i}\gamma_3}\left(\frac{\gamma_4\gamma_6^*}{E_{c+2}-E_c}+\frac{\gamma_4\gamma_6^*}{E_{c+2}-E_v}-\frac{\gamma_5\gamma_2^*}{E_v-E_{v-3}}-\frac{\gamma_5\gamma_2^*}{E_c-E_{v-3}}\right). \tag{19}$$

Equations (18) can be conveniently derived taking into account the interband matrix elements of the dipole moment operator contain both $\boldsymbol{k}$-independent and $\boldsymbol{k}$-linear terms as

$$-(\boldsymbol{d}\cdot\boldsymbol{e})^{(+)}=-\frac{\mathrm{i}\sqrt{2}e\gamma_3}{E_g}\left(e_-+\mathrm{i}Ak_+e_+\right), \tag{20a}$$

$$-(\boldsymbol{d}\cdot\boldsymbol{e})^{(-)}=+\frac{\mathrm{i}\sqrt{2}e\gamma_3^*}{E_g}\left(e_++\mathrm{i}A^*k_-e_-\right), \tag{20b}$$

where the superscript $(\pm)$ denotes the valley where the interband transition takes place.

Hence, for example, both $2s$-shell exciton formed with the electron in the $\boldsymbol{K}_+$ valley and $2p_-$-shell exciton formed with the electron in the $\boldsymbol{K}_-$ valley are active in the same polarization. As a result, these state become mixed via the electromagnetic field induced by the excitons. Microscopically, this mixing can be attributed to the long-range exchange interaction between the electron and hole forming the exciton [26, 32]. Below we evaluate the mixing both in the electrodynamical and quantum-mechanical approaches and discuss its specifics as compared with the short-range exchange contribution presented above.

In the framework of the electrodynamical approach we evaluate the interaction of the exciton with the induced electromagnetic field. As before, we focus on $2s$- and $2p$-shell states. It is instructive to consider the excitons propagating with the wavevector $\boldsymbol{K}\parallel x$ in the TMD ML plane excited by the plane wave with the frequency ω, the wavevector components $q_x=K$, $q_y=0$, $q_z=\sqrt{(n\omega/c)^2-K^2}$, and the field components $E^0_{x,y}$, n is the refraction index of TMD ML. The exciton-induced field is found from the Maxwell equations [26, 32, 37]:

$$E_x=E_x^0+\frac{q_z}{q}\mathrm{i}G\left(\frac{|\gamma_3\Phi_{2s}|^2}{\omega_{2s}-\omega-\mathrm{i}\Gamma}+\frac{|A\gamma_3\Phi'_{2p}|^2}{\omega_{2p}-\omega-\mathrm{i}\Gamma}\right)E_x, \tag{21a}$$

$$E_y=E_y^0+\frac{q}{q_z}\mathrm{i}G\left(\frac{|\gamma_3\Phi_{2s}|^2}{\omega_{2s}-\omega-\mathrm{i}\Gamma}+\frac{|A\gamma_3\Phi'_{2p}|^2}{\omega_{2p}-\omega-\mathrm{i}\Gamma}\right)E_y, \tag{21b}$$

where to shorten the notations the argument $\rho=0$ is omitted, $\omega_\nu=E_\nu/\hbar$, Γ is the non-radiative damping of the exciton (its difference for the s- and p-shell excitons is disregarded), $q=n\omega/c$, and G is the factor depending of the dielectric surrounding of the TMD ML, it can be expressed via the electromagnetic Greens function. Formally, the mechanical exciton energies in Eqs. (21) should include the contributions of the short-range exchange interaction which already mixes the s- and p-shell states. The analysis of the interference of the short- and long-range exchange mechanisms is beyond the scope of the present paper. From the consistency requirement of Eqs. (21) we obtain the following equations for the exciton eigenfrequencies:

$$(\omega_{2p}-\mathrm{i}\Gamma-\lambda_\alpha\Gamma_{0,2p})(\omega_{2s}-\mathrm{i}\Gamma-\lambda_\alpha\Gamma_{0,2s})=-\lambda_\alpha^2\Gamma_{0,2s}\Gamma_{0,2p}, \tag{22}$$

where the subscript $\alpha=x,y$, the factors $\lambda_x=q_z/q$, $\lambda_y=q/q_z$, and we introduced the radiative decay rates of the $2s$- and $2p$-shell excitons as

$$\Gamma_{0,2s}=G|\gamma_3\Phi_{2s}|^2,\quad \Gamma_{0,2p}=G|\gamma_3 A\Phi'_{2p}|^2. \tag{23}$$

Note that the parameter G is real and positive, and $0<\Gamma_{0,2p}\ll\Gamma_{0,2s}$, the latter inequality holds because with the $\boldsymbol{k}\cdot\boldsymbol{p}$ approach the $|A|/a_B\ll 1$.

Equation (22) demonstrates that the coupling between s- and p-shell excitons is "dissipative" for the states with the wavevectors within the light cone, $K<n\omega/c$. Formally this is because for real q_z the right-hand side of Eq. (22) is negative and the coupling constants $\beta_{l,\alpha}=\mathrm{i}\lambda_\alpha\hbar\sqrt{\Gamma_{0,2s}\Gamma_{0,2p}}$ are imaginary. Physically, the excitons with $K<n\omega/c$ emit propagating electromagnetic waves, which results in the exciton damping, correspondingly, the mixing between the $2s$ and $2p$ excitons is also associated with their damping. This is quite similar to the situation of the polarization-dependent renormalization of the exciton radiative damping for the s-shell exciton states within the light cone [26, 32].

The situation is different for the excitonic states outside the light cone where $K>n\omega/c$. Such excitons do not emit propagating electromagnetic waves and s-p-shell states coupling is produced by the curl-less (longitudinal) electromagnetic field. Hence, the coupling constants β_α are real and the maximal coupling is achieved for the longitudinal exciton, $\alpha=x$:

$$\beta_{l,x}=\frac{c\hbar K}{n\omega}\Gamma_{0,2s}\frac{|A\Phi'_{2p}|}{|\Phi_{2s}|},\quad \beta_{l,y}\ll\beta_{l,x}, \tag{24}$$

where we assumed $K\gg n\omega/c$. Note that if the excitons are localized as a whole by a shallow in-plane potential the mixing constant can be estimated by means of Eq. (24) replacing K by the inverse localization length [44].

Equation (24) can be also derived quantum mechanically taking into account the long-range exchange interaction between the electron and the hole. To that end,

let us first consider the interband scattering of two electrons from the states $c\boldsymbol{k}_c$ and $v\boldsymbol{k}_v$ to the states $v\boldsymbol{k}'_v$ and $c\boldsymbol{k}'_c$. The matrix element of this process is given by

$$V_{exch} = \left\langle \mathcal{U}^{(+)}_{c,\boldsymbol{k}'_c}(\boldsymbol{\rho}_2)\mathcal{U}^{(-)}_{v,\boldsymbol{k}'_v}(\boldsymbol{\rho}_1)\right| V_c \left|\mathcal{U}^{(-)}_{c,k_c}(\boldsymbol{\rho}_1)\mathcal{U}^{(+)}_{v,\boldsymbol{k}_v}(\boldsymbol{\rho}_2)\right\rangle, \tag{25}$$

where $V_c = V_c(\boldsymbol{\rho}_1 - \boldsymbol{\rho}_2)$ is the Coulomb interaction between the electrons. This matrix element differs from the matrix element of the direct interaction by a substitution $\boldsymbol{\rho}_1 \leftrightarrow \boldsymbol{\rho}_2$ in the initial or final state. The specifics of TMD ML is that the interacting electrons are in different valleys. By contrast to Eqs. (13), (16) here we are interested in the long-range part of the Coulomb interaction, which allows to rearrange Eq. (25) as

$$V_{exch} = \left\langle \mathcal{U}^{(+)}_{c,\boldsymbol{k}'_c}\middle|\mathcal{U}^{(+)}_{v,\boldsymbol{k}_v}\right\rangle \left\langle \mathcal{U}^{(-)}_{v,\boldsymbol{k}'_v}\middle|\mathcal{U}^{(-)}_{c,\boldsymbol{k}_c}\right\rangle V_c(\boldsymbol{k}_c - \boldsymbol{k}'_v) \times \delta_{\boldsymbol{k}_c-\boldsymbol{k}'_v,\boldsymbol{k}'_c-\boldsymbol{k}_v}, \tag{26}$$

where

$$V_c(\boldsymbol{K}) = \frac{2\pi e^2}{n^2 K}, \tag{27}$$

is the Fourier image of the Coulomb interaction. Note that the screening of the long-range exchange interaction is realized by the high-frequency dielectric constant [26]. The overlap integrals of the Bloch functions are non-zero if the $\boldsymbol{k}\cdot\boldsymbol{p}$ mixing of the conduction and valence bands is taken into account in the first order, cf. Eq. (12):

$$\left\langle \mathcal{U}^{(+)}_{c,\boldsymbol{k}'_c}\middle|\mathcal{U}^{(+)}_{v,\boldsymbol{k}_v}\right\rangle = \frac{\gamma_3}{E_g}\left[K_- + \mathrm{i}AK_+\frac{(k'_c + k_v)_+}{2}\right], \tag{28a}$$

$$\left\langle \mathcal{U}^{(-)}_{v,\boldsymbol{k}'_v}\middle|\mathcal{U}^{(-)}_{c,\boldsymbol{k}_c}\right\rangle = -\frac{\gamma_3}{E_g}\left[K_- + \mathrm{i}AK_+\frac{(k'_c + k_v)_+}{2}\right], \tag{28b}$$

with $\boldsymbol{K} = \boldsymbol{k}'_c - \boldsymbol{k}_v = \boldsymbol{k}_c - \boldsymbol{k}'_v$. Evaluation of Eq. (25) by virtue of Eqs. (26) and (28) and transformation to the electron-hole representation yields Eq. (24). Note that to obtain the general expression for the $2s$-$2p$ exciton mixing for the whole range of the wavevectors including those within the light cone, one has to take into account the retardation of Coulomb interaction [50]. To that end it is sufficient to use, instead of Eq. (27), the general form of the retarded potential taken at $z = 0$

$$V_c = \int_{-\infty}^{\infty}\frac{dk_z}{2\pi}\frac{4\pi e^2}{n^2[K^2 + k_z^2 - (n\omega/c)^2]} = \frac{2\pi e^2}{n^2\sqrt{K^2 - (n\omega/c)^2}}.$$

For the states within the light cone, $K \to 0$, the efficiency of the dissipative s-p mixing can be estimated according to Eqs. (22) and (23) as $|\beta_l| \sim \hbar\Gamma_{0s}|A|/a_B \sim \hbar\Gamma_{0s}a_0/a_B \sim 0.1\ldots1$ meV depending on the particular material [51] and dielectric environment which is close to the estimates in Sec. (III B) for the short-range mixing mechanism. The coupling constant is enhanced by the factor $K/(n\omega/c) > 1$ for the states outside of the light cone, see Eq. (24).

IV. NONLINEAR OPTICAL PROPERTIES OF EXCITONS IN TMD MLs

In this section we address the consequences of the three-fold symmetry of TMD ML, particularly, the intrinsic exciton mixing on the excitonic nonlinear optical properties, namely, in the two-photon absorption and in the second harmonic generation. It is commonly accepted that the s-shell exciton states are active in single-photon absorption, while p-shell states are active in the two-photon processes [38]. The lack of spatial inversion in TMD MLs enables single-photon excitation of p-shell excitons and two-photon excitation of s-shell excitons. There are two mechanisms of the selection rules modification: (i) $\boldsymbol{k}$-linear terms in the interband dipole matrix elements, Eqs. (20), and (ii) the mixing of excitonic states of different parity described by the parameter β in Eq. (6). As a result, each s-shell and p-shell exciton state become simultaneously single- and two-photon active, resulting in the second harmonic generation. Below we consider both mechanisms of the nonlinear excitonic response.

A. Modification of the dipole matrix elements due to k-linear terms

The physical origin of the two-photon excitation of s-shell excitons is illustrated in Fig. 4 for the particular case of the $1s$ exciton. In this two-stage process the single-photon excitation of the $2p$-exciton takes place owing to $\boldsymbol{k}$-linear terms in Eq. (20). The second photon absorption goes through the inter-exciton transition [38, 52], which changes the envelope function parity $\langle ns|x\mp\mathrm{i}y|mp_\pm\rangle \neq 0$. Hence, the s-shell excitonic states $\Psi_{\mathbf{0};ns;+1}$ are excited by two σ^- polarized photons, while the states $\Psi_{\mathbf{0};ns;-1}$ are excited by two σ^+ polarized photons.

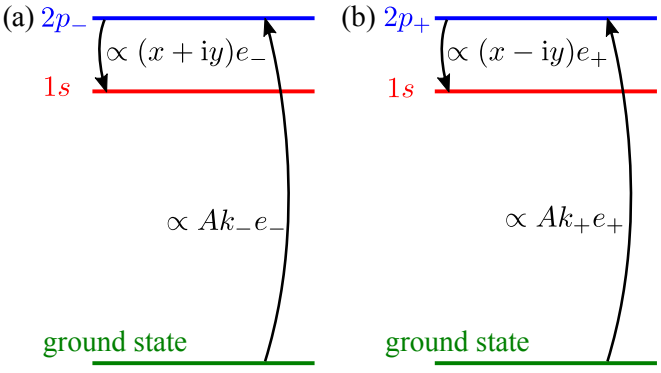

Figure 4. Demonstration of the two-photon activity of the $1s$-exciton due to $\boldsymbol{k}$-linear terms in the interband dipole matrix element, Eq. (20). In this mechanism the mixing of excitons is not required. Panels (a) and (b) show the exciton states with the electron in $\boldsymbol{K}_-$ and $\boldsymbol{K}_+$ valley, respectively.

Taking into account that the $\boldsymbol{k}$-linear terms in the interband matrix element result from the $\boldsymbol{k}\cdot\boldsymbol{p}$ interac-

tion with remote, $c+2$ and $v-3$ bands, one can see that the two-photon excitation of s-shell excitons takes place via two "allowed" transitions, i.e., $v \to c+2$ and $c+2 \to c$ or $v \to v-3$ and $v-3 \to c$. Under the assumptions that the exciton binding energy $E_b \ll E_g$ and that $E_v - E_{v-3}, E_{c+2} - E_c \gg E_g$ the two-photon transition matrix element can be calculated neglecting the Coulomb interaction and averaged over the exciton wavefunction afterwards. The composite matrix element of the two-photon transition takes the form [53]

$$M^{(2)} = \left(\frac{e}{\omega}\right)^2 \sum_m \frac{(\boldsymbol{E}\cdot\hat{\boldsymbol{v}})_{cm}(\boldsymbol{E}\cdot\hat{\boldsymbol{v}})_{mv}}{E_m - E_v - \hbar\omega}, \tag{29}$$

where the summation takes place over intermediate states ($m = c+2$ and $v-3$ for the $c \to v$ transition), $\hat{\boldsymbol{v}}$ is the velocity operator, $\boldsymbol{E}$ is the complex amplitude of the electric field in the incident wave. For the $c \to v$ two-photon transition at the $\boldsymbol{K}_+$ point one has from Eq. (29) neglecting $\hbar\omega = E_g/2$ as compared with $E_v - E_{v-3}, E_{c+2} - E_c$

$$M^{(2,+)} = \left(\frac{e}{\omega}\right)^2 \frac{\mathrm{i}\gamma_3}{\hbar} A E_{\sigma^-}^2, \tag{30}$$

where $E_{\sigma^\mp}$ are the corresponding circular components of the incident field and A is given by Eq. (19). In agreement with the fact that both steps are "allowed" the composite matrix element, Eq. (30), is independent of the wavevector. As a result, s-shell excitons with even envelope functions can be excited in the two-photon process. Similarly to the case of the direct interband transitions the matrix element of the two-photon excitation of the ns-exciton state is given by Eq. (30) multiplied by $\Phi^*_{ns}(0)$ (the normalization area is set to 1):

$$M^{(2,+)}_{ns} = \left(\frac{e}{\omega}\right)^2 \frac{\mathrm{i}\gamma_3}{\hbar} A \Phi^*_{ns}(0) E_{\sigma^-}^2. \tag{31}$$

Analogously, one can derive the expression for the matrix element $M^{(2,-)}_{ns}$ of the two-photon excitation by σ^+ polarized light, it differs from Eq. (31) by the replacement E_{σ^-} by E_{σ^+} and the complex conjugation of the product $\mathrm{i}\gamma_3 A$.

The possibility of the two-photon excitation of ns states leads to the electro-dipole second harmonic generation. Phenomenologically, the second harmonic generation in D_{3h} point symmetry is described by the relation [20, 54–56]

$$P_x^{(2\omega)} = 2\chi^{(2)} E_x E_y, \quad P_y^{(2\omega)} = \chi^{(2)}(E_x^2 - E_y^2), \tag{32}$$

Here $\chi^{(2)}$ is the only allowed component of the second order susceptiblity. For the sake of simplicity we focus on the experimentally relevant case of the second harmonic generation at $1s$ exciton. Making use of Eqs. (31) and (17) we arrive at the following expression for the susceptibility $\chi^{(2)}$ related with $\boldsymbol{k}$-linear terms in the dipole matrix elements:

$$\chi^{(2)}_{k,1s} = -\frac{e^3|\Phi_{1s}(0)|^2}{\omega^2\omega_{1s}} A \left|\frac{\gamma_3}{\hbar}\right|^2 \frac{1}{2\omega - \omega_{1s} + \mathrm{i}\Gamma_{1s}}, \tag{33}$$

where Γ_{1s} is the damping of the $1s$ exciton state. Clearly, $\chi^{(2)}_{k,1s}$ has a resonance at $\omega = \omega_{1s}/2$ where the double frequency corresponds to the $1s$ exciton frequency in which case the real part of the denominator $2\omega - \omega_{1s} + \mathrm{i}\Gamma_{1s}$ vanishes. Analogous expressions for the second-order susceptibility can be derived for ω in the vicinity of any s-shell excitonic resonance.

We note that the two-photon excitation of the p-shell excitons does not require a lack of an inversion center and takes place via a combination of the "allowed" interband and "forbidden" intraband transitions [38, 52]. Taking into account that the intraband matrix elements of the velocity operator read $\boldsymbol{v}_{cc} = \hbar k/m_c$, $\boldsymbol{v}_{vv} = \hbar k/m_v$, where $m_{c,v}$ are the effective masses of the electron in the conduction and valence bands, respectively, and $1/m_c - 1/m_v = 1/\mu$ where μ is the reduced electron-hole mass we obtain from Eq. (29)

$$\tilde{M}^{(2,+)} = \left(\frac{e}{\omega}\right)^2 \frac{\gamma_3}{\omega\mu} k_+ E_{\sigma^-}^2. \tag{34}$$

As compared with Eq. (30) for the two-step process involving intra- and interband transitions the effective two-photon matrix element is linear in the wavevector $\boldsymbol{k}$. That is why p-shell excitons are optically active in the two-photon processes and the matrix element of the two-photon excitation of the mp-exciton state is given, in accordance with Eq. (34) by

$$\tilde{M}^{(2,+)}_{mp} = \left(\frac{e}{\omega}\right)^2 \frac{-\mathrm{i}\gamma_3}{\omega\mu} \left[\Phi'_{mp}(0)\right]^* E_{\sigma^-}^2. \tag{35}$$

Due to the lack of an inversion symmetry the p-shell excitons are optically active in single photon processes. Taking into account Eqs. (18) we have for the contribution to the susceptibility related with the $2p$-exciton

$$\chi^{(2)}_{k,2p} = \frac{e^3\hbar|\Phi'_{2p}(0)|^2}{\mu\omega^3\omega_{2p}} A^* \left|\frac{\gamma_3}{\hbar}\right|^2 \frac{1}{2\omega - \omega_{2p} + \mathrm{i}\Gamma_{2p}}. \tag{36}$$

It is worth stressing that the susceptibility is proportional to the parameter A (A^*) responsible for the lack of the inversion center in TMD ML.

Let us compare the contributions Eq. (33) and (36) to the nonlinear susceptibility at $1s$ and $2p$ excitons. Taking into account that $|\Phi'_{2p}(0)|^2 \sim a_B^{-2}|\Phi_{1s}(0)|^2$ and $\hbar^2/\mu a_B^2 \sim E_b$ we observe that the ratio of the peak values of $\chi^{(2)}$ can be estimated as

$$\frac{\chi^{(2)}_{k,1s}(\omega = \omega_{1s})}{\chi^{(2)}_{k,2p}(\omega = \omega_{2p})} \sim \frac{E_g}{E_b}\frac{\Gamma_{2p}}{\Gamma_{1s}} \gg 1. \tag{37}$$

The dominance of the $1s$ exciton contribution is related with two large factors, $\hbar\omega/E_b \sim E_g/E_b > 1$ and $\Gamma_{2p}/\Gamma_{1s} > 1$ because the broadening of the excited states exceeds by far the broadening of the ground exciton state [20].

B. Mixing of excitons

The mixing of the s- and p-shell excitons described by the Hamiltonian (6) gives rise to additional contributions to the two-photon absorption by s-shell exciton states and to the second order susceptibility. These nonlinear contributions are similar to those related with the magneto-Stark-effect or electric-field induced mixing of excitons in ZnO and GaAs [57, 58]. Schematically, one of these contributions is illustrated in Fig. 5: the p-shell exciton can be excited in a one photon process due to admixture $\propto \beta$ of the s-shell state, the absorption of the second photon transforms, as in the previous section, the p-shell exciton to the s-shell one.

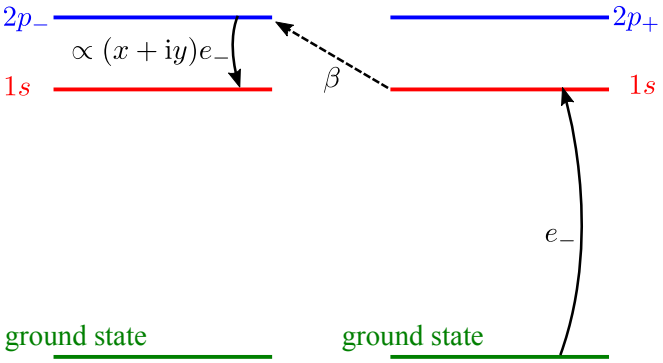

Figure 5. Demonstration of the two-photon activity of the $1s$-exciton due to the p-s-exciton mixing, Eq. (6). Left and right show the exciton states with the electron in $\boldsymbol{K}_-$ and $\boldsymbol{K}_+$ valley, respectively. Dashed arrows denote the mixing of excitonic states of different parity.

Microscopically, the response of the TMD ML taking into account the exciton mixing can be derived similarly to the two-photon activity of the $2p$ excitons, because the two-photon excitation of the s-shell state takes place via a combination of the interband and intraband processes. Taking into account that the wavefunction of the s-shell state contains $\propto \beta$ admixture of the p-shell states the averaging of Eq. (34) produces a non-zero result for s-shell excitons. Omitting the details of derivation we present the final result for the $1s$ exciton contribution to $\chi^{(2)}$ related with the $1s$-mp exciton mixing:

$$\chi^{(2)}_{\beta,1s} = -\frac{e^3\hbar\Phi_{1s}(0)}{\mu\omega^3\omega_{1s}}\left|\frac{\gamma_3}{\hbar}\right|^2\sum_m \frac{\beta_{1m}[\Phi'_{mp}(0)]^*}{E_{1s}-E_{mp}}\times \frac{1}{2\omega-\omega_{1s}+i\Gamma_{1s}}. \quad (38)$$

The resonance in Eq. (38) takes place, as in Eq. (33), at $\omega = \omega_{1s}/2$ when the second harmonic is resonant with the $1s$ exciton state. Similar expressions can be derived for the contributions to the nonlinear susceptibility $\chi^{(2)}$ in the vicinity of other excitonic resonances. For instance, the second harmonic generation at p-shell excitons is related with the standard mechanism of the two-photon excitation of the p-shell, Eq. (35), and single-photon emission from the p-exciton due to $\propto \beta$ admixture of the s-shell state to the p-shell state. Here lack of the inversion center is accounted for by the s-p exciton mixing constants β_{1m}.

C. Discussion and comparison with experiment

A giant enhancement of the second harmonic generation at exciton resonances in 1 ML WSe_2 flakes has been observed in Ref. [20]. The monolayer samples were obtained by micromechanical cleavage of bulk WSe_2 crystal on 90 nm SiO_2 on a Si substrate. For the two-photon excitation we use picosecond light pulses, generated by a tunable optical parametric oscillator synchronously pumped by a mode-locked Ti:sapphire laser. The second harmonic emission was collected in reflection geometry, see Ref. [20] for details. Figure 6 demonstrates the intensity of the second harmonic signal as a function of the doubled laser excitation energy. A strong peak at $1s$ exciton is clearly seen as well as less prominent feature at the $2s/2p$ excitons. The peaks at exciton resonances in the second-order susceptibility are in agreement with the developed model.

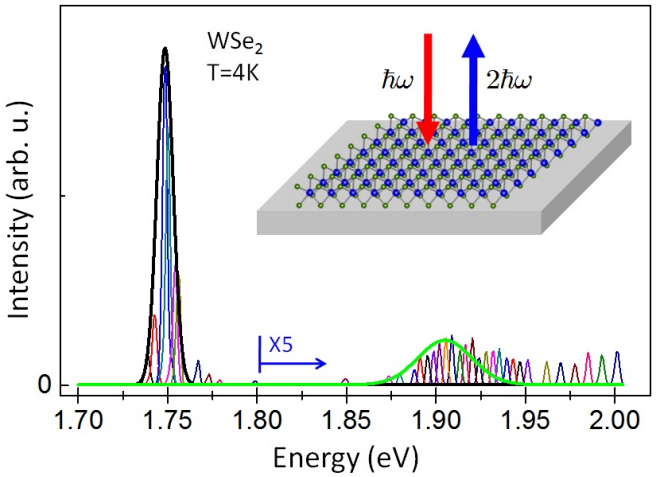

Figure 6. The second harmonics generation spectrum at $T = 4$ K as function of two photon energy, $2\hbar\omega$. Narrow peaks represent the emission intensity measured at a given laser frequency. Solid black and green lines represent the fits with Gauss function to the $1s$ and $2s/2p$ transition profiles. The inset shows the the schematics of the experiment. Adapted from Ref. [20].

The dominant second harmonic response at the $1s$ exciton state can be explained within the developed model accounting for the modification of the matrix elements, Sec. IV A. The estimates by Eqs. (33), (37) show that $1s$ exciton should dominate in the second harmonic emission. As compared with all excited states the ground exciton has much smaller broadening, moreover, the $2s$ state has much smaller oscillator strength

$|\Phi_{2s}(0)/\Phi_{1s}(0)|^2 \ll 1$ already in the hydrogenic model, while as compared with $2p$ exciton the enhancement is caused by the factor E_b/E_g. To provide more quantitative comparison we fitted the spectra of the second harmonic generation at $1s$ and $2s/2p$ excitons by Gaussian functions (see black and green profiles in Fig. 6) and extracted the ratio of the integral second harmonic intensities at $1s$ and $2s/2p$ states to be about 10. We abstain from more detailed fitting of the experimental data with our model due to uncertainty of the sample parameters and difficulties with evaluation of the overall emission intensity in such samples, cf. [59]. This is in reasonable agreement with the first factor in Eq. (37), $E_g/E_b \sim 5$ in WSe_2. It demonstrates that the mechanism related with the modification of selection rules, Eqs. (33), (36), already reproduces all main features of the experiment.

V. CONCLUSION

In the present paper we have developed the theory of the excitonic states fine structure in transition metal dichalcogenides monolayers. We have demonstrated that the lack of inversion center in the TMD MLs and their specific three-fold rotation symmetry gives rise to the mixing of the exciton states with different parity. In particular, s-shell and p-shell excitonic states whose two-dimensional envelope functions are characterized by the angular momentum components 0 and ±1 are coupled in TMD MLs. The microscopic theory of the mixing is developed with the $\boldsymbol{k}\cdot\boldsymbol{p}$ formalism. We have identified the origins of the mixing related with the long- and short-range parts of the electron-hole exchange interaction. The estimates show that the coupling constant for the nearest $2s$-$2p$ or $1s$-$2p$ states may be in the range of tenths to units of meV.

The manifestations of the exciton mixing in the linear and, especially, nonlinear optical properties are studied. We have demonstrated that in TMD MLs s-shell excitons are allowed not only in single-photon but also in two-photon processes. Similarly, p-shell excitons are active in single-photon absorption in addition to the two-photon absorption. We have shown that, besides exciton mixing, the lack of the inversion center in TMD MLs results in the modification of optical selection rules, which also provides simultaneous activity of s- and p-shell excitons in one- and two-photon processes. These mechanisms give rise to the effective generation of the crystallographic second harmonics in the electro-dipole approximation. The mechanism related with the modification of the selection rules provides dominant second harmonic response at $1s$-exciton resonance in qualitative agreement with experiment.

The precise evaluation of the exciton oscillator strengths and the nonlinear susceptibility by the combination of the $\boldsymbol{k}\cdot\boldsymbol{p}$ model developed here and the atomistic calculations as well as the studies of the interplay of the exciton mixing in absence and in presence of an external electric field are the tasks for future studies.

ACKNOWLEDGMENTS

We are grateful for partial support to RFBR, the Russian Federation President Grant MD-5726.2015.2, Dynasty foundation, LIA CNRS-Ioffe RAS ILNACS, ERC Grant No. 306719, and ANR MoS2ValleyControl for financial support. X.M. also acknowledges the Institut Universitaire de France.

Appendix A: Derivation of Eqs. (10) and (12)

We start from the electron-hole pair with the wavevectors $\boldsymbol{k}_e$ and $\boldsymbol{k}_h$. The Bloch function of this pair (without the Coulomb interaction) reads

$$\Psi_{\boldsymbol{k}_e,\boldsymbol{k}_h}(\boldsymbol{\rho}_e,\boldsymbol{\rho}_h) = e^{\mathrm{i}\boldsymbol{k}_e\boldsymbol{\rho}_e+\mathrm{i}\boldsymbol{k}_h\boldsymbol{\rho}_h}\mathcal{U}_{c,\boldsymbol{k}_e}(\boldsymbol{\rho}_e)\tilde{\mathcal{U}}_{v,\boldsymbol{k}_h}(\boldsymbol{\rho}_h). \quad \text{(A1)}$$

Here $\boldsymbol{\rho}_e$ and $\boldsymbol{\rho}_h$ are the in-plane position vectors of the electron and the hole, $\mathcal{U}_{c,\boldsymbol{k}_e}(\boldsymbol{\rho}_e)$ $[\tilde{\mathcal{U}}_{v,\boldsymbol{k}_h}(\boldsymbol{\rho}_h)]$ are the single particle Bloch functions for the conduction band electron (valence band hole). The normalization area is set to unity. In the first order in the $\boldsymbol{k}\cdot\boldsymbol{p}$ mixing we have for the Bloch functions

$$\mathcal{U}_{c,\boldsymbol{k}_e}(\boldsymbol{\rho}_e) = \mathcal{U}_{c,\boldsymbol{k}_e=0}(\boldsymbol{\rho}_e) + \sum_m \mathcal{U}_{m,0}(\boldsymbol{\rho}_e)\frac{\frac{\hbar}{m_0}\langle m|\boldsymbol{k}_e\cdot\boldsymbol{p}|c\rangle}{E_c-E_m}, \quad \text{(A2)}$$

$$\tilde{\mathcal{U}}_{v,\boldsymbol{k}_h}(\boldsymbol{\rho}_e) = \tilde{\mathcal{U}}_{v,\boldsymbol{k}_h=0}(\boldsymbol{\rho}_e) + \sum_n \tilde{\mathcal{U}}_{n,0}(\boldsymbol{\rho}_e)\frac{\frac{\hbar}{m_0}\langle n|\boldsymbol{k}_h\cdot\boldsymbol{p}|c\rangle}{E_c-E_n}. \quad \text{(A3)}$$

The wavevectors are reckoned from the corresponding $\boldsymbol{K}$ point of the Brillouin zone, e.g., $\boldsymbol{k}_e = 0$ corresponds to $\boldsymbol{K}_+$ valley for the electron and $\boldsymbol{k}_h = 0$ corresponds to the $\boldsymbol{K}_-$ valley for the hole in the electron-hole pair excited by the σ^+ light.

Now we account for the excitonic effect. We assume that the exciton binding energy is small as compared with the bandgaps and include the Coulomb correlation in the form

$$\Psi_{exc}(\boldsymbol{\rho}_e,\boldsymbol{\rho}_h) = \sum_{\boldsymbol{k}_e,\boldsymbol{k}_h} C_{\boldsymbol{k}_e,\boldsymbol{k}_h} e^{\mathrm{i}\boldsymbol{k}_e\boldsymbol{\rho}_e+\mathrm{i}\boldsymbol{k}_h\boldsymbol{\rho}_h}\mathcal{U}_{c,\boldsymbol{k}_e}(\boldsymbol{\rho}_e)\tilde{\mathcal{U}}_{v,\boldsymbol{k}_h}(\boldsymbol{\rho}_h). \quad \text{(A4)}$$

Here $C_{\boldsymbol{k}_e,\boldsymbol{k}_h}$ is the Fourier transform of the exciton envelope function calculated within the effective mass approach,

$$\exp(\mathrm{i}\boldsymbol{K}\boldsymbol{R})\Phi(\boldsymbol{\rho}_e-\boldsymbol{\rho}_h) = \sum_{\boldsymbol{k}_e,\boldsymbol{k}_h} C_{\boldsymbol{k}_e,\boldsymbol{k}_h} e^{\mathrm{i}\boldsymbol{k}_e\boldsymbol{\rho}_e+\mathrm{i}\boldsymbol{k}_h\boldsymbol{\rho}_h}. \quad \text{(A5)}$$

Hence, in the first order in the $\boldsymbol{k}\cdot\boldsymbol{p}$ mixing one has

$$\Psi_{exc}(\boldsymbol{\rho}_e,\boldsymbol{\rho}_h) = \sum_{\boldsymbol{k}_e,\boldsymbol{k}_h} C_{\boldsymbol{k}_e,\boldsymbol{k}_h} e^{\mathrm{i}\boldsymbol{k}_e\boldsymbol{\rho}_e+\mathrm{i}\boldsymbol{k}_h\boldsymbol{\rho}_h}\mathcal{U}_{c,0}(\boldsymbol{\rho}_e)\tilde{\mathcal{U}}_{v,0}(\boldsymbol{\rho}_h)+ \delta\Psi_e(\boldsymbol{\rho}_e)\tilde{\mathcal{U}}_{v,0}(\boldsymbol{\rho}_h)+\delta\Psi_h(\boldsymbol{\rho}_h)\mathcal{U}_{c,0}(\boldsymbol{\rho}_e). \quad \text{(A6)}$$

Making use of Eq. (A2) we have for $\delta\Psi_e$:

$$\delta\Psi_e(\boldsymbol{\rho}_e) = \quad \text{(A7)}$$

$$\sum_{\boldsymbol{k}_e,\boldsymbol{k}_h} C_{\boldsymbol{k}_e,\boldsymbol{k}_h} e^{\mathrm{i}\boldsymbol{k}_e\boldsymbol{\rho}_e+\mathrm{i}\boldsymbol{k}_h\boldsymbol{\rho}_h}\sum_m \mathcal{U}_{m,0}(\boldsymbol{\rho}_e)\frac{\frac{\hbar}{m_0}\langle m|\boldsymbol{k}_e\cdot\boldsymbol{p}|c\rangle}{E_c-E_m} =$$

$$\sum_{\boldsymbol{k}_e,\boldsymbol{k}_h} C_{\boldsymbol{k}_e,\boldsymbol{k}_h} e^{\mathrm{i}\boldsymbol{k}_e\boldsymbol{\rho}_e+\mathrm{i}\boldsymbol{k}_h\boldsymbol{\rho}_h} k_-^{(e)}\left[\frac{\gamma_6\mathcal{U}^{(e)}_{c+2}(\boldsymbol{\rho}_e)}{E_c-E_{c+2}}+\frac{\gamma_5^*\mathcal{U}^{(e)}_{v-3}(\boldsymbol{\rho}_e)}{E_c-E_{v-3}}\right].$$

In the latter equality we have considered the particular case of the electron in the $\boldsymbol{K}_+$ valley and took into account two admixed bands, $c+2$ and $v-3$ where

$$\frac{\hbar}{m_0}\langle c+2|\boldsymbol{k}_e\cdot\boldsymbol{p}|c\rangle=\gamma_6 k_-^{(e)}, \quad \frac{\hbar}{m_0}\langle v-3|\boldsymbol{k}_e\cdot\boldsymbol{p}|c\rangle=\gamma_5^* k_-^{(e)}.$$

To sum over $\boldsymbol{k}_e,\boldsymbol{k}_h$ in Eq. (A7) we consider the exciton with the center of mass wavevector $\boldsymbol{K}=0$ and make use of Eq. (A5) to obtain

$$\sum_{\boldsymbol{k}_e,\boldsymbol{k}_h} C_{\boldsymbol{k}_e,\boldsymbol{k}_h} e^{\mathrm{i}\boldsymbol{k}_e\boldsymbol{\rho}_e+\mathrm{i}\boldsymbol{k}_h\boldsymbol{\rho}_h} k_-^{(e)} \quad \text{(A8)}$$

$$= \sum_{\boldsymbol{k}_e,\boldsymbol{k}_h} C_{\boldsymbol{k}_e,\boldsymbol{k}_h}(-\mathrm{i})\left(\frac{\partial}{\partial x_e}-\mathrm{i}\frac{\partial}{\partial y_e}\right)e^{\mathrm{i}\boldsymbol{k}_e\boldsymbol{\rho}_e+\mathrm{i}\boldsymbol{k}_h\boldsymbol{\rho}_h}$$

$$= -\mathrm{i}\left(\frac{\partial}{\partial x_e}-\mathrm{i}\frac{\partial}{\partial y_e}\right)\Phi(\boldsymbol{\rho}_e-\boldsymbol{\rho}_h)=\hat{k}_-\Phi(\boldsymbol{\rho}).$$

Combining Eqs. (A6), (A7) and (A8) we obtain Eq. (10) of the manuscript with the function $\mathcal{W}_-$ in the form

$$\mathcal{W}_- = \left(\frac{\gamma_6\mathcal{U}^{(+)}_{c+2}(\boldsymbol{\rho}_e)}{E_c-E_{c+2}}+\frac{\gamma_5^*\mathcal{U}^{(+)}_{v-3}(\boldsymbol{\rho}_e)}{E_c-E_{v-3}}\right)\tilde{\mathcal{U}}_v^{(-)}(\boldsymbol{\rho}_h).$$

This is the first line of Eq. (12a). The second line of Eq. (12a) can be derived in the same way from $\delta\Psi_h$ in Eq. (A6).

[1] Kin Fai Mak, Changgu Lee, James Hone, Jie Shan, and Tony F. Heinz, "Atomically thin MoS_2: A new direct-gap semiconductor," Phys. Rev. Lett. **105**, 136805 (2010).

[2] Di Xiao, Gui-Bin Liu, Wanxiang Feng, Xiaodong Xu, and Wang Yao, "Coupled spin and valley physics in monolayers of MoS_2 and other group-VI dichalcogenides," Phys. Rev. Lett. **108**, 196802 (2012).

[3] Qing Hua Wang, Kourosh Kalantar-Zadeh, Andras Kis, Jonathan N. Coleman, and Michael S. Strano, "Electronics and optoelectronics of two-dimensional transition metal dichalcogenides," Nat. Nano. **7**, 699–712 (2012).

[4] Gui-Bin Liu, Di Xiao, Yugui Yao, Xiaodong Xu, and Wang Yao, "Electronic structures and theoretical modelling of two-dimensional group-VIB transition metal dichalcogenides," Chem. Soc. Rev. **44**, 2643–2663 (2015).

[5] Alexander V. Kolobov and Junji Tominaga, *Two-Dimensional Transition-Metal Dichalcogenides* (Springer International Publishing, 2016).

[6] Hongyi Yu, Xiaodong Cui, Xiaodong Xu, and Wang Yao, "Valley excitons in two-dimensional semiconductors," National Science Review **2**, 57–70 (2015).

[7] Galan Moody, John Schaibley, and Xiaodong Xu, "Exciton dynamics in monolayer transition metal dichalcogenides," J. Opt. Soc. Am. B **33**, C39–C49 (2016).

[8] A. V. Chaplik and M. V. Entin, "Charged impurities in very thin layers," JETP **34**, 1335 (1972).

[9] L. V. Keldysh, "Coulomb interaction in thin semiconductor and semimetal films," JETP Lett. **29**, 658 (1979).

[10] Tawinan Cheiwchanchamnangij and Walter R. L. Lambrecht, "Quasiparticle band structure calculation of monolayer, bilayer, and bulk MoS_2," Phys. Rev. B **85**, 205302 (2012).

[11] Ashwin Ramasubramaniam, "Large excitonic effects in monolayers of molybdenum and tungsten dichalcogenides," Phys. Rev. B **86**, 115409 (2012).

[12] Hongliang Shi, Hui Pan, Yong-Wei Zhang, and Boris I. Yakobson, "Quasiparticle band structures and optical properties of strained monolayer MoS_2 and WS_2," Phys. Rev. B **87**, 155304 (2013).

[13] Diana Y. Qiu, Felipe H. da Jornada, and Steven G. Louie, "Optical spectrum of MoS_2 many-body effects and diversity of exciton states," Phys. Rev. Lett. **111**, 216805 (2013).

[14] Gunnar Berghäuser and Ermin Malic, "Analytical approach to excitonic properties of MoS_2," Phys. Rev. B **89**, 125309 (2014).

[15] Kin Fai Mak, Keliang He, Changgu Lee, Gwan Hyoung Lee, James Hone, Tony F. Heinz, and Jie Shan, "Tightly bound trions in monolayer MoS_2," Nat Mater **12**, 207–211 (2013).

[16] Keliang He, Nardeep Kumar, Liang Zhao, Zefang Wang, Kin Fai Mak, Hui Zhao, and Jie Shan, "Tightly bound excitons in monolayer WSe_2," Phys. Rev. Lett. **113**, 026803 (2014).

[17] Alexey Chernikov, Timothy C. Berkelbach, Heather M. Hill, Albert Rigosi, Yilei Li, Ozgur Burak Aslan,

David R. Reichman, Mark S. Hybertsen, and Tony F. Heinz, "Exciton binding energy and nonhydrogenic rydberg series in monolayer WS_2," Phys. Rev. Lett. **113**, 076802 (2014).
[18] Ziliang Ye, Ting Cao, Kevin O'Brien, Hanyu Zhu, Xiaobo Yin, Yuan Wang, Steven G. Louie, and Xiang Zhang, "Probing excitonic dark states in single-layer tungsten disulphide," Nature **513**, 214–218 (2014).
[19] A. R. Klots, A. K. M. Newaz, Bin Wang, D. Prasai, H. Krzyzanowska, Junhao Lin, D. Caudel, N. J. Ghimire, J. Yan, B. L. Ivanov, K. A. Velizhanin, A. Burger, D. G. Mandrus, N. H. Tolk, S. T. Pantelides, and K. I. Bolotin, "Probing excitonic states in suspended two-dimensional semiconductors by photocurrent spectroscopy," Sci. Rep. **4** (2014).
[20] G. Wang, X. Marie, I. Gerber, T. Amand, D. Lagarde, L. Bouet, M. Vidal, A. Balocchi, and B. Urbaszek, "Giant enhancement of the optical second-harmonic emission of WSe_2 monolayers by laser excitation at exciton resonances," Phys. Rev. Lett. **114**, 097403 (2015).
[21] T. Korn, S. Heydrich, M. Hirmer, J. Schmutzler, and C. Schüller, "Low-temperature photocarrier dynamics in monolayer MoS_2," Applied Physics Letters **99**, 102109 (2011).
[22] G. Wang, L. Bouet, D. Lagarde, M. Vidal, A. Balocchi, T. Amand, X. Marie, and B. Urbaszek, "Valley dynamics probed through charged and neutral exciton emission in monolayer WSe_2," Phys. Rev. B **90**, 075413 (2014).
[23] Maurizia Palummo, Marco Bernardi, and Jeffrey C. Grossman, "Exciton radiative lifetimes in layered transition metal dichalcogenides," Nano Letters **15**, 2794 (2015).
[24] C. Poellmann, P. Steinleitner, U. Leierseder, P. Nagler, G. Plechinger, M. Porer, R. Bratschitsch, C. Schuller, T. Korn, and R. Huber, "Resonant internal quantum transitions and femtosecond radiative decay of excitons in monolayer WSe_2," Nat Mater **14**, 889 (2015).
[25] C. Robert, D. Lagarde, F. Cadiz, G. Wang, B. Lassagne, T. Amand, A. Balocchi, P. Renucci, S. Tongay, B. Urbaszek, and X. Marie, "Exciton radiative lifetime in transition metal dichalcogenide monolayers," Phys. Rev. B **93**, 205423 (2016).
[26] M. M. Glazov, T. Amand, X. Marie, D. Lagarde, L. Bouet, and B. Urbaszek, "Exciton fine structure and spin decoherence in monolayers of transition metal dichalcogenides," Phys. Rev. B **89** (2014).
[27] T. Yu and M. W. Wu, "Valley depolarization due to intervalley and intravalley electron-hole exchange interactions in monolayer MoS_2," Phys. Rev. B **89**, 205303 (2014).
[28] Hongyi Yu, Gui-Bin Liu, Pu Gong, Xiaodong Xu, and Wang Yao, "Dirac cones and Dirac saddle points of bright excitons in monolayer transition metal dichalcogenides," Nat. Commun. **5** (2014).
[29] Diana Y. Qiu, Ting Cao, and Steven G. Louie, "Nonanalyticity, valley quantum phases, and lightlike exciton dispersion in monolayer transition metal dichalcogenides: Theory and first-principles calculations," Phys. Rev. Lett. **115**, 176801 (2015).
[30] J. P. Echeverry, B. Urbaszek, T. Amand, X. Marie, and I. C. Gerber, "Splitting between bright and dark excitons in transition metal dichalcogenide monolayers," Phys. Rev. B **93**, 121107 (2016).
[31] C. R. Zhu, K. Zhang, M. Glazov, B. Urbaszek, T. Amand, Z. W. Ji, B. L. Liu, and X. Marie, "Exciton valley dynamics probed by Kerr rotation in WSe_2 monolayers," Phys. Rev. B **90**, 161302 (2014).
[32] M. M. Glazov, E. L. Ivchenko, G. Wang, T. Amand, X. Marie, B. Urbaszek, and B. L. Liu, "Spin and valley dynamics of excitons in transition metal dichalcogenide monolayers," physica status solidi (b) **252**, 2349–2362 (2015).
[33] K. L. Seyler, J. R. Schaibley, P. Gong, P. Rivera, A. M. Jones, S. Wu, J. Yan, D. G. Mandrus, W. Yao, and X. Xu, "Electrical control of second-harmonic generation in a WSe_2 monolayer transistor", Nat. Nano. **10**, 407 (2015).
[34] Mads L. Trolle, Yao-Chung Tsao, Kjeld Pedersen, and Thomas G. Pedersen, "Observation of excitonic resonances in the second harmonic spectrum of MoS_2," Phys. Rev. B **92**, 161409 (2015).
[35] Mads L. Trolle, Gotthard Seifert, and Thomas G. Pedersen, "Theory of excitonic second-harmonic generation in monolayer MoS_2," Phys. Rev. B **89**, 235410 (2014).
[36] G. L. Bir, G. E. Pikus, *Symmetry and Strain-induced Effects in Semiconductors* (Wiley/Halsted Press, 1974).
[37] E. L. Ivchenko, *Optical spectroscopy of semiconductor nanostructures* (Alpha Science, Harrow UK, 2005).
[38] Timothy C. Berkelbach, Mark S. Hybertsen, and David R. Reichman, "Bright and dark singlet excitons via linear and two-photon spectroscopy in monolayer transition-metal dichalcogenides," Phys. Rev. B **92**, 085413 (2015).
[39] Ajit Srivastava and Atac Imamoglu, "Signatures of bloch-band geometry on excitons: Nonhydrogenic spectra in transition-metal dichalcogenides," Phys. Rev. Lett. **115**, 166802 (2015).
[40] Jianhui Zhou, Wen-Yu Shan, Wang Yao, and Di Xiao, "Berry phase modification to the energy spectrum of excitons," Phys. Rev. Lett. **115**, 166803 (2015).
[41] A. O. Slobodeniuk and D. M. Basko, "Spin-flip processes and radiative decay of dark intravalley excitons in transition metal dichalcogenide monolayers," arXiv:1603.02572 (2016).
[42] George F. Koster, Robert G. Wheeler, John O. Dimmock, and Hermann Statz, *Properties of the thirty-two point groups* (MIT Press, 1963).
[43] Fengcheng Wu, Fanyao Qu, and A. H. MacDonald, Exciton band structure of monolayer MoS_2, Phys. Rev. B **91**, 075310 (2015).
[44] M. M. Glazov, E. L. Ivchenko, R. von Baltz, and E. G. Tsitsishvili, "Fine structure of excited excitonic states in quantum dots," Int. J. Nanoscience **6**, 265 (2007).
[45] Andor Kormányos, Viktor Zólyomi, Neil D. Drummond, Péter Rakyta, Guido Burkard, and Vladimir I. Fal'ko, "Monolayer MoS_2: Trigonal warping, the γ valley, and spin-orbit coupling effects," Phys. Rev. B **88**, 045416 (2013).
[46] Andor Kormanyos, Guido Burkard, Martin Gmitra, Jaroslav Fabian, Viktor Zólyomi, Neil D Drummond, and Vladimir Fal'ko, "$\boldsymbol{k}\cdot\boldsymbol{p}$ theory for two-dimensional transition metal dichalcogenide semiconductors," 2D Materials **2**, 022001 (2015).
[47] G. Wang, L. Bouet, M. M. Glazov, T. Amand, E. L. Ivchenko, E. Palleau, X. Marie, and B. Urbaszek, "Magneto-optics in transition metal diselenide monolayers," 2D Materials **2**, 034002 (2015).
[48] Kin Fai Mak, Keliang He, Jie Shan, and Tony F. Heinz, "Control of valley polarization in monolayer MoS_2 by optical helicity," Nat. Nano. **7**, 494–498 (2012).

[49] G. Sallen, L. Bouet, X. Marie, G. Wang, C. R. Zhu, W. P. Han, Y. Lu, P. H. Tan, T. Amand, B. L. Liu, and B. Urbaszek, "Robust optical emission polarization in mos_2 monolayers through selective valley excitation," Phys. Rev. B **86**, 081301 (2012).

[50] S. V. Goupalov, E. L. Ivchenko, and A. V. Kavokin, "Fine structure of localized exciton levels in quantum wells," JETP **86**, 388 (1998).

[51] D. V. Rybkovskiy, I. C. Gerber, and M. V. Durnev, "Atomically inspired $k \cdot p$ approach and valley Zeeman effect in transition metal dichalcogenide monolayers," arXiv:1610.02695 (2016).

[52] G. D. Mahan, "Theory of two-photon spectroscopy in solids," Phys. Rev. **170**, 825–838 (1968).

[53] E. L. Ivchenko, "Two-photon absorption and optical orientation of free carriers in cubic crystals", Sov. Phys. Solid State **14**, 2942 (1973).

[54] L. E. Golub, S. A. Tarasenko, M. V. Entin, and L. I. Magarill, "Valley separation in graphene by polarized light," Phys. Rev. B **84**, 195408 (2011).

[55] M.M. Glazov and S.D. Ganichev, "High frequency electric field induced nonlinear effects in graphene," Physics Reports **535**, 101 (2014).

[56] L. E. Golub and S. A. Tarasenko, "Valley polarization induced second harmonic generation in graphene," Phys. Rev. B **90**, 201402 (2014).

[57] M. Lafrentz, D. Brunne, B. Kaminski, V. V. Pavlov, A. V. Rodina, R. V. Pisarev, D. R. Yakovlev, A. Bakin, and M. Bayer, "Magneto-stark effect of excitons as the origin of second harmonic generation in ZnO," Phys. Rev. Lett. **110**, 116402 (2013).

[58] D. Brunne, M. Lafrentz, V. V. Pavlov, R. V. Pisarev, A. V. Rodina, D. R. Yakovlev, and M. Bayer, "Electric field effect on optical harmonic generation at the exciton resonances in GaAs," Phys. Rev. B **92**, 085202 (2015).

[59] D.-H. Lien, J. S. Kang, M. Amani, K. Chen, M. Tosun, H.-P. Wang, T. Roy, M. S. Eggleston, M. C. Wu, M. Dubey, S.-C. Lee, J.-H. He, and A. Javey, "Engineering light outcoupling in 2D materials," Nano Letters **15**, 1356 (2015).